ROZPRAWY INŻYNIERSKIE • ENGINEERING TRANSACTIONS • 26, 3, 471—500, 1978
Polska Akademia Nauk • Instytut Podstawowych Problemów Techniki

PRECISE MEASUREMENT AND FORMULATION OF PLASTIC BEHAVIOUR OF METALS

Y. OHASHI (NAGOYA)

In the present paper, results of investigations on the plastic behaviour under complex-loading by using an automatic complex-loading testing machine are summarized in accordance with the data obtained in our laboratory. Some experimental results on mild steel subjected to proportional deformations under combined loadings of axial force, torque and internal pressure applied to thin-walled tubular specimens with constant strain rate are discussed with emphasis on the effects of the first and third invariants of stress and strain. Experimental results under the above-mentioned combined loadings are discussed further on the plastic behaviour along the strain trajectories with a right-angle corner in the three-dimensional vector space corresponding to strain deviator. As the results of these experiments, the relations between stress and strain after the corner of strain trajectories which are in the relation of mirror transformation do not always agree with each other. However, such a disagreement for the relations almost vanishes after a modification in which the effect of the third invariant is eliminated from the experimental results. In other words, Ilyushin's "postulate of isotropy" is satisfied almost completely after such a modification on the results obtained by the above-mentioned experiments for mild steel. After such a modification, experimental relations between stress and strain after the corner of strain trajectory are formulated in a form of nonlinear tensor equality.

1. Introduction

Complicated nonlinear phenomena accompanying history effects appear in the plastic deformation of real materials, and thus it has been very difficult, from the mathematical standpoint, to reffect them properly in deformation analyses. To avoid these difficulties, an elegant "plastic flow theory" which is convenient for mathematical analysis has been formulated by neglecting the complicated history effects which appear in real materials. The results of these developments have been described in a variety of books, including the famous treaties by R. Hill [1], and represent a considerable contribution to the analysis of plastic deformation. However, this simplified theory is able to approximate only a part of the plastic behaviour of real materials under complicated loading systems; still, it is applicable in a wide range of engineering problems. For this reason, various investigations have been conducted to modify this plastic flow theory so as to reflect the history effects [2–8]. However, there remain many difficulties, both thoeretical and practical.

The reason why the flow theory cannot express precisely the plastic behaviour due to strongly varying history effects seems to be that an irreversible process in the plastic deformation, which should be considered as the so-called path-dependent

one, has been approximated by introducing the "plastic potential" which is by nature a path-independent function. Even for a comparatively mild history effect it would be difficult to determine precisely the functions expressing a sequence of innumerable potential surfaces along a complex loading path from the corresponding calibration tests.

Since most of the mathematical difficulties have been eliminated by the introduction of computers, it may be said that the accuracy of an analytical result mainly depends on the approximation in formulating the results of precise observation of deformation behaviours of real materials under complex loading systems.

In the field of continuum mechanics, a general form of constitutive equation has been constructed in terms of functionals concerning the characteristics of deformation behaviour which materials acquire through the history effects [9]. The general plastic theory in a five-dimensional vector space corresponding to a stress or strain deviator proposed by ILYUSHIN [10] in formulating plastic behaviours of metals under complex loading also belongs to this category, and his "postulate of isotropy" and "principle of delay" also seem to be useful approximations to simplify the constitutive equation being considered generally in the field of continuum mechanics. His theory has been discussed experimentally by LENSKY [11] who veriefied the validity of this theory for some metals under certain complex loading systems.

However, as IVLEV [12] and NOVOZHILOV [13] have pointed out, the vector space used by Ilyushin cannot reflect explicitly some of the characteristics in tensor space.

Under circumstances such as those mentioned above, a full-automatic complex-loading testing machine with high accuracy was constructed recently in our laboratory for the precise measurement of the plastic behaviour of metals subjected to combined loadings.

Using this apparatus in the first experiment, proportional deformations under combined loading were measured with high accuracy on mild steel. From the results it was ascertained that the third invariant of strain (or stress) deviator affects the experimental results considerably, whereas the first invariant does little. These invariants cannot be expressed explicitely in the vector space.

Next, as a fundamental example of plastic behaviour under complex loading, experiments were performed with a constant strain rate along various kinds of strain trajectories consisting of two straight segments intersecting so as to form a corner. In the results of the precise measurements of deformation behaviours for mild steel, the history effect on the deformation behaviour along the trajectory after the corner was mingled with the effect of the third invariant mentioned above. Thus, the postulate of isotropy in the vector space could not be satisfied accurately on the basis of the experimental results obtained for the effect of the third invariant.

However, by modifying the vector space to eliminate the effect of the third invariant from the measured value, plastic behaviours after the corner on mild steel may be expressed by an identical stress-strain relation for a fixed geometry of strain trajectory, respectively irrespective of the orientation in the vector space.

Moreover, the distribution of the third invariant was found in the vector space, and the relation between stress and strain-increment deviators, which are not coaxial in general, was formulated in the form of a nonlinear tensor equation. The relation may express the deformation behaviour after the corner with high accuracy.

2. Specimen [14, 15] and experimental apparatus [14]

The specimen is a thin-walled tubular specimen precisely machined from a bar of initially isotropic mild steel (S10C). The apparatus is an automatic complex loading testing machine which can apply combined loadings of axial force, torque and internal pressure precisely to the above mentioned specimen with automatic control. It also records the values of load and deformation simultaneously.

3. General relation between deviatoric tensors [16]

In the consideration of deformation properties of materials with regard to stress and strain or strain-increment as tensor quantities, the properties may be expressed by the functional relations between these tensors. Moreover, as the relation between their spherical parts may be regarded as elastic, the inelastic properties of the materials may be discussed as to the relation between their deviators.

The resulting variation in deformation properties after various plastic deformations of initially isotropic materials, that is the history effect in deformation properties, may be formulated in the form of a tensorial functional relation between the above-mentioned deviators in the isotropic deviatoric space.

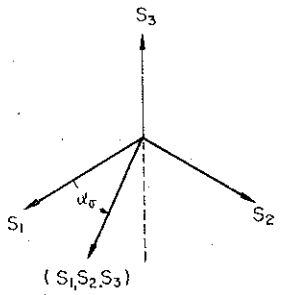

Fig. 1. Plane of stress deviator D_σ: s_i $(i=1, 2, 3)$ denotes the principal values of D_σ.

In order to formulate rationally the experimental results in the most general form, the relation between a stress deviator $D_\sigma=(s_{ij}\, e_i\, e_j;\quad i, j=1, 2, 3)$ and a strain-increment deviator $D_{de}=(de_{ij}\, e_i\, e_j$, $i, j=1, 2, 3)$ is derived, for example, where e_i $(i=1, 2, 3)$ denote the base vectors which prescribe the space, $e_i e_j$ denote the corresponding base tensors, and s_{ij} de_{ij} are the corresponding components. When a set of orthonormal base vectors concerning the principal directions of D_σ is selected as e_i' $(i=1, 2, 3)$, the trigonometric form of D_σ may be expressed as

$$D_\sigma=s_{ij}\, e_i\, e_j=(2/\sqrt{3})\,\zeta_\sigma\{\cos\alpha_\sigma\, e_1' e_1'-\cos(\alpha_\sigma+\pi/3)\, e_2' e_2'-\cos(\alpha_\sigma-\pi/3)\, e_3' e_3'\}, \tag{3.1a}$$

$$\zeta_\sigma^2=\mathrm{tr}(D_\sigma^2)/2\equiv I_2(D_\sigma),\qquad \cos 3\alpha_\sigma=(3\sqrt{3}/2)\, I_3(D_\sigma)/I_2(D_\sigma)^{3/2}=(3\sqrt{3}/2)\, I_3(D_\sigma)/\zeta_\sigma^3, \tag{3.1b}$$

$$I_3(D_\sigma)\equiv\mathrm{tr}(D_\sigma^3)/3,$$

where $I_2(D_\sigma)$ and $I_3(D_\sigma)$ denote the second and third invariants of the stress deviator D_σ, respectively, and α_σ denotes an angle expressing the stress state (ref. Fig. 1).

In terms of three deviatoric base tensors with respect to the stress deviator

$$
\begin{aligned}
&\mathsf{G}_1=\sqrt{2}/3\delta_{ij}\,\mathsf{e}'_i\,\mathsf{e}'_j\,(i,j=1,2,3),\\
&\mathsf{G}_2=(1/\sqrt{3}\,(2\mathsf{e}'_1\,\mathsf{e}'_1-\mathsf{e}'_2\,\mathsf{e}'_2-\mathsf{e}'_3\,\mathsf{e}'_3),\\
&\mathsf{G}_3=\mathsf{e}'_2\,\mathsf{e}'_2-\mathsf{e}'_3\,\mathsf{e}'_3,
\end{aligned}
\tag{3.2}
$$

which are mutually orthonormal, the expression (3.1a) may be rewritten in the following form:

$$
\mathsf{D}_\sigma=\zeta_\sigma(\cos\alpha_\sigma\,\mathsf{G}_2+\sin\alpha_\sigma\,\mathsf{G}_3)\,. \tag{3.3}
$$

In the same way D_{de} may be expressed in terms of a set of orthonormal base vectors d_i $(i=1, 2, 3)$ for the principal directions of D_{de} in the following form:

$$
\begin{aligned}
&\mathsf{D}_{de}=\zeta_{de}(\cos\alpha_{de}\,\mathsf{H}_2+\sin\alpha_{de}\,\mathsf{H}_3),\\
&\zeta^2_{de}=\mathrm{tr}\,(\mathsf{D}^2_{de})/2=I_2\,(\mathsf{D}_{de}),\\
&\cos 3\alpha_{de}=(3\sqrt{3}/2)\,I_3(\mathsf{D}_{de})/I_2\,(\mathsf{D}_{de})^{3/2}=(3\sqrt{3}/2)\,I_3\,(\mathsf{D}_{de})/\zeta^3_{de},\\
&I_3\,(\mathsf{D}_{de})\equiv\mathrm{tr}\,(\mathsf{D}^3_{de})/3,
\end{aligned}
\tag{3.4}
$$

where $I_2\,(\mathsf{D}_{de})$ and $I_3\,(\mathsf{D}_{de})$ denote the second and third invariants of the strain-increment deviator D_{de}, respectively, and α_{de} denotes an angle expressing the strain-increment state.

$$
\begin{aligned}
&\mathsf{H}_1=\sqrt{2/3}\,\delta_{ij}\,\mathsf{d}_i\,\mathsf{d}_j\,(i,j=1,2,3), \qquad \mathsf{H}_2=(1/\sqrt{3})\,(2\mathsf{d}_1\,\mathsf{d}_1-\mathsf{d}_2\,\mathsf{d}_2-\mathsf{d}_3\,\mathsf{d}_3),\\
&\mathsf{H}_3\equiv\mathsf{d}_2\,\mathsf{d}_2-\mathsf{d}_3\,\mathsf{d}_3
\end{aligned}
\tag{3.5}
$$

are designated as base tensors for the principal directions of the strain-increment deviator D_{de}, which are orthonormal with each other.

Since the principal directions of D_σ and D_{de} are not always coaxial in general plastic deformation, the above-mentioned two sets of base tensors G_i and H_i $(i=1, 2, 3)$ may differ from each other. Since the functional relation between the deviators D_σ and D_{de} should be derived on common bases, the deviator D_{de} is expressed with respect to the base G_i of D_σ.

By introducing a rotation tensor L of orthogonal systems such as

$$
\mathsf{e}'_i=\mathsf{L}\,\mathsf{d}_i \qquad (i=1, 2, 3) \tag{3.6}
$$

and using the relation $\mathsf{e}'_i\,\mathsf{e}'_j=\mathsf{L}\mathsf{d}_i\,\mathsf{d}_j\,\mathsf{L}^{-1}$ or $\mathsf{d}_i\,\mathsf{d}_j=\mathsf{L}^{-1}\,\mathsf{e}'_i\,\mathsf{e}'_j\,\mathsf{L}$, the following relation is obtained:

$$
\mathsf{H}_i=\mathsf{L}^{-1}\,\mathsf{G}_i\,\mathsf{L} \qquad (i=1, 2, 3). \tag{3.7}
$$

By substituting the relation (3.7) into Eqs. (3.4a), a form is obtained in which D_{de} is expressed with respect to the orthonormal base tensor G_i for the deviator D_σ as follows,

$$
\mathsf{L}\mathsf{D}_{de}\,\mathsf{L}^{-1}/\zeta_{de}=\cos\alpha_{de}\,\mathsf{G}_2+\sin\alpha_{de}\,\mathsf{G}_3\,. \tag{3.8}
$$

In order to construct the base tensors G_2 and G_3 with two tensors which are not mutually coaxial, a quadratic deviator of $LD_{de}L^{-1}/\zeta_{de}$

$$(LD_{de}L^{-1}/\zeta_{de})^2-\sqrt{2/3}\,G_1=LD_{de}^2L^{-1}/\zeta_{de}^2-\sqrt{2/3}\,G_1= \\ =(1/\sqrt{3})(\cos 2\alpha_{de}G_2-\sin 2\alpha_{de}G_3) \tag{3.9}$$

may be selected as the simplest normalized tensor which is not coaxial with $LD_{de}L^{-1}/\zeta_{de}$. In this respect the relations between the orthonormal base tensors

$$G_2G_2=\sqrt{2/3}\,G_1+(1/\sqrt{3})G_2, \qquad G_2G_3=G_3G_2=-(1/\sqrt{3})G_3, \\ G_3G_3=\sqrt{2/3}\,G_1-(1/\sqrt{3})G_2, \tag{3.10}$$

found from the relations (3.2) were used.

The following expressions are derived from Eqs. (3.8) and (3.9):

$$\sin 3\alpha_{de}G_3=\cos 2\alpha_{de}(LD_{de}L^{-1}/\zeta_{de})-3\cos\alpha_{de}(LD_{de}^2L^{-1}/\zeta_{de}^2-\sqrt{2/3}\,G_1), \\ \sin 3\alpha_{de}G_2=\sin 2\alpha_{de}(LD_{de}L^{-1}/\zeta_{de})+3\sin\alpha_{de}(LD_{de}^2L^{-1}/\zeta_{de}^2-\sqrt{2/3}\,G_1). \tag{3.11}$$

In the case of $\sin 3\alpha_{de}\neq 0$, the following relation between stress and strain-increment deviators may be obtained by substituting G_2 and G_3 from Eqs. (3.11) into Eq. (3.3):

$$D_\sigma/\zeta_\sigma=(1/\sin 3\alpha_{de})\{\sin(2\alpha_{de}+\alpha_\sigma)LD_{de}L^{-1}/\zeta_{de}+ \\ +\sqrt{3}\sin(\alpha_{de}-\alpha_\sigma)(LD_{de}^2L^{-1}/\zeta_{de}^2-\sqrt{2/3}\,G_1)\}. \tag{3.12}$$

When the deviators D_σ and D_{de} are coaxial, the rotation tensor L is reduced to the unit tensor I and the well-known relation is obtained as follows [17]:

$$D_\sigma/\zeta_\sigma=(1/\sin 3\alpha_{de})\{\sin(2\alpha_{de}+\alpha_\sigma)D_{de}/\zeta_{de}+ \\ +\sqrt{3}\sin(\alpha_{de}-\alpha_\sigma)(D_{de}^2/\zeta_{de}^2-\sqrt{2/3}\,G_1)\}. \tag{3.13}$$

In the case of $\alpha_\sigma=\alpha_{de}$ in Eq. (3.13), the relation between D_σ and D_{de} is reduced to the linear relation corresponding to the St. Venant-Levy-Mises law used conventionally:

$$D_\sigma=(\zeta_\sigma/\zeta_{de})D_{de}. \tag{3.14}$$

In the case of $\sin 3\alpha_{de}=0$, the following relation is obtained from Eqs. (3.11):

$$\pm LD_{de}L^{-1}/\zeta_{de}=3(LD_{de}^2L^{-1}/\zeta_{de}^2-\sqrt{2/3}\,G_1).$$

Thus the quadratic deviator cannot be used as the base tensor. In such a case the deviator D_σ may be expressed in the following form by selecting $LD_{de}L^{-1}/\zeta_{de}$ and G_3 as base tensors, for example,

$$D_\sigma=\zeta_\sigma\{\cos\alpha_\sigma(LD_{de}L^{-1}/\zeta_{de})+\sin\alpha_\sigma G_3\}. \tag{3.15}$$

4. Deviatoric strain vector space and deviatoric stress vector space

As shown in Eqs. (31b) or (3.4b), each third invariant depends on the angle α_σ or α_{de}. The angle α_σ or α_{de} expresses the state of D_σ or D_{de}, i.e. the relation between the elements of the deviator. For convenience this relation may be expressed geometrically in the corresponding vector space. Since geometric representation is very effective in discussing the history effect on the deformation behaviour of materials, the behaviour is expressed in the vector spaces corresponding to the deviatoric tensor space. In this respect special case must be taken in expressing experimental results, because the first and third invariants of the tensor cannot be expressed explicitly in the vector space while the second one can be expressed.

A strain deviator $D_e=e_{ij}\,e_i\,e_j$ $(i,j=1,2,3)$ may be expanded as follows:

$$D_e=e_k A_k \qquad (1,2,\ldots,5), \tag{4.1}$$

with respect to five orthonormal base tensors:

$$A_k=A^k_{ij}\,e_i\,e_j \qquad (k=1,2,\ldots,5; \quad i,j=1,2,3).$$

The scalar coefficients e_k have the following relation in connection with e_{ij}:

$$e_{ij}=e_k A^k_{ij} \qquad (i,j=1,2,3; \quad k=1,2,\ldots,5). \tag{4.2}$$

The relation

$$e_{ij}e_{ij}=e_k e_k \qquad (i,j=1,2,3; \quad k=1,2,\ldots,5) \tag{4.3}$$

together with

$$\begin{gathered}\sqrt{3/2}\,e_{mm}=B_{mk}e_k \qquad (m=1,2,3 \text{ are not summed}; \quad k=1.2),\\ \sqrt{2}\,e_{12}=e_3, \qquad \sqrt{2}\,e_{23}=e_4, \qquad \sqrt{2}\,e_{31}=e_5\end{gathered} \tag{4.4}$$

is designated between the second invariant in the deviatoric tensor space and the invariant in the corresponding vector space where B_{mk} are scalar coefficients.

The following relations hold between e_k and e_{ij}:

$$\begin{aligned}e_1&=\sqrt{2}\,\{e_{11}\cos(\gamma+\pi/6)-e_{22}\sin\gamma\},\\ e_2&=\sqrt{2}\,\{e_{11}\sin(\gamma+\pi/6)+e_{22}\cos\gamma\},\\ e_3&=\sqrt{2}\,e_{12}, \qquad e_4=\sqrt{2}\,e_{23}, \qquad e_5=\sqrt{2}\,e_{31}.\end{aligned} \tag{4.5}$$

On the other hand, the following expressions are obtained for the base tensors: A_k $(k=1,2,\ldots,5)$.

$$\begin{aligned}A_1&=\sqrt{2/3}\,\{\cos\gamma\,e_1\,e_1-\sin(\gamma+\pi/6)\,e_2\,e_2+\sin(\gamma-\pi/6)\,e_3\,e_3\},\\ A_2&=\sqrt{2/3}\,\{\sin\gamma\,e_1\,e_1+\cos(\gamma+\pi/6)\,e_2\,e_2-\cos(\gamma-\pi/6)\,e_3\,e_3\},\\ A_1&=\sqrt{2/3}\cos\pi/6)(e_1\,e_2+e_2\,e_1), \qquad A_4=\sqrt{2/3}\cos(\pi/6)(e_2\,e_3+e_3\,e_2),\\ A_5&=\sqrt{2/3}\cos(\pi/6)(e_3\,e_1+e_1\,e_3),\end{aligned} \tag{4.6}$$

where γ is an arbitrary parameter. From Eqs. (4.6) the base tensors A_k are found to be orthonormal.

From Eqs. (4.1), (4.5) and (4.6) the state of deviatoric strain corresponding to D_e may be expressed by the coefficients e_l $(i=1, 2, ..., 5)$ by using the base tensors A_k constructed from a set of suitably prescribed orthonormal base vectors e_l. Thus the deviatoric strain vector

$$\mathsf{e}=e_k \mathsf{n}_k \quad \text{for } (k=1, 2, ..., 5), \quad (\mathsf{n}_k\text{: orthonormal base vectors}) \tag{4.7}$$

may be introduced for the state of deviatoric strain corresponding to D_e, if a five-dimensional vector space V_{5e} of the deviatoric strain

$$\begin{aligned}[e_1, e_2, ..., e_5]=[&\sqrt{2}\,\{e_{11}\cos(\gamma+\pi/6)-e_{22}\sin\gamma\},\\ &\sqrt{2}\,\{e_{11}\sin(\gamma+\pi/6)+e_{22}\cos\gamma\}, \quad \sqrt{2}\,e_{12}, \quad \sqrt{2}\,e_{23}, \quad \sqrt{2}\,e_{31}],\end{aligned} \tag{4.8}$$

is used. This vector space has been introduced by ILYUSHIN [10].

By an approximation that the plane stress state appears in the tubular specimen, if the axis-3 is selected in the radial direction of the specimen, the components of stress σ_{i3} $(i=1, 2, 3)$ and strain ε_{i3} $(i=1, 2)$ vanish, and thus the axis-3 becomes a fixed principal axis for the stress deviator D_σ or strain deviator D_e. Then D_e may be expressed as follows for $\gamma=0$:

$$\begin{aligned}&\mathsf{D}_e=e_k \mathsf{A}_k, \quad (k=1, 2, 3),\\ &\mathsf{D}_e=\sqrt{3/2}\,[e_{11}\{\sqrt{2/3}\,(\mathsf{e}_1\mathsf{e}_1-\mathsf{e}_2\mathsf{e}_2/2-\mathsf{e}_3\mathsf{e}_3/2)\}+(2/\sqrt{3})(e_{11}/2+\\ &\qquad +e_{22})\{\sqrt{1/2}\,\mathsf{e}_2\mathsf{e}_2-\mathsf{e}_3\mathsf{e}_3)\}+(2/\sqrt{3})e_{12}\sqrt{1/2}\,(\mathsf{e}_1\mathsf{e}_2+\mathsf{e}_2\mathsf{e}_1)].\end{aligned} \tag{4.9}$$

Accordingly, the state of deviatoric strain corresponding to D_e given in Eq. (4.9) may be expressed by a strain vector

$$\mathsf{e}=e_{11}\mathsf{n}_1+(2/\sqrt{3})(e_{11}/2+e_{22})\mathsf{n}_2+(2/\sqrt{3})\,\mathsf{e}_{12}\mathsf{n}_3, \tag{4.10}$$

in a three-dimensional vector space V_{3e}

$$[e_1, e_2, e_3]=[e_{11}, \quad (2/\sqrt{3})(e_{11}/2+e_{22}), \quad (2/\sqrt{3})e_{12}]. \tag{4.11}$$

The history of deviatoric strain may be expressed by a hodograph of the strain vector e (strain trajectory) in the space V_{3e}.

The state of deviatoric stress at an arbitrary point on the strain trajectory may be expressed by a deviatoric stress vector

$$\boldsymbol{\sigma}=(3/2)\{s_{11}\mathsf{n}_1+(2/\sqrt{3})(s_{11}/2+s_{22})\mathsf{n}_2+(2/\sqrt{3})s_{12}\mathsf{n}_3\} \tag{4.12}$$

in a local vector space $V_{3\sigma}$

$$[\sigma_1, \sigma_2, \sigma_3]=[(3/2)s_{11}, \sqrt{3}\,(s_{11}/2+s_{22}), \sqrt{3}\,s_{12}], \tag{4.13}$$

corresponding to the deviatoric stress established at that point where s_{ij} $(i, j=1, 2, 3)$ are components of D_σ, and σ_k $(k=1, 2, 3)$ denote the components introduced for D_σ in the same way as in the relation (4.1).

In the representation (4.9), if the base vector $\mathbf{e}_1$ and $\mathbf{e}_2$ rotate orthogonally around the base vector $\mathbf{e}_3$ corresponding to the fixed principal axis of D_e, the components e_{11}, e_{22}, and e_{12} of the D_e vary so as to correespond to the basis after rotation, and the strain vector $\mathbf{e}$ also rotates around the origin in the space V_{3e}. Thus, a history of a deviatoric strain state given in the space established with the base tensor A_k ($k=1, 2, 3$) may correspond to a set of strain trajectories in the space V_{3e}. In other words, the strain trajectories in such a set may be equivalent to each other in that space yet still be different in orientation. On the other hand, the strain trajectories which are equivalent tensorially may be confirmed to have an identical geometry in the space V_{3e}. Still, every strain trajectory having the same geometry is not always equivalent tensorially.

The magnitude $|\mathbf{e}|$ and direction (φ_e, θ_e) of the deviatoric strain vector $\mathbf{e}$ in the space $V_3 e$ and the magnitude $|\boldsymbol{\sigma}|$ and direction $(\varphi_k, \theta_\sigma)$ of the deviatoric stress vector $\boldsymbol{\sigma}$ in the local space $V_3 \sigma$ appearing in (4.10) through (4.13) are expressed as

$$|\mathbf{e}|=(e_1^2+e_2^2+e_3^2)^{1/2}=\{e_{11}^2+(4/3)(e_{11}/2+e_{22})^2+(4/3)e_{12}^2\}^{1/2}, \tag{4.14}$$

$$\tan\varphi_e=e_2/e_1=(e_{11}+2e_{22})/\sqrt{3}\,e_{11}, \qquad \cos\theta_e=\mathbf{e}\cdot\mathbf{n}_3/|\mathbf{e}|=2e_{12}/\sqrt{3}\,|\mathbf{e}|,$$

$$|\boldsymbol{\sigma}|=\sigma_1^2+\sigma_2^2+\sigma_3^2)^{1/2}=(3/2)\{s_{11}^2+(4/3)(s_{11}/2+s_{22})^2+(4/3)s_{12}^2\}^{1/2}, \tag{4.15}$$

$$\tan\varphi_\sigma=\sigma_2/\sigma_1=(s_{11}+2s_{22})/\sqrt{3}\,s_{11}, \qquad \cos\theta_\sigma=\boldsymbol{\sigma}\cdot\mathbf{n}_3/|\boldsymbol{\sigma}|=\sqrt{3}\,s_{12}/|\boldsymbol{\sigma}|.$$

As found from Eqs. (4.14) and (4.15) the magnitude $|\mathbf{e}|$ and $|\boldsymbol{\delta}|$ agree with the equivalent strain and the equivalent stress, respectively.

5. Distributions of the first and third invariants on the three-dimensional vector space [16, 19]

Since the second invariant $I_2(\mathsf{D})$ of the deviatoric tensor is maintained in the corresponding vector space introduced in the previous section, the magnitude of $I_2(\mathsf{D})$ is kept constant at every point on the spherical surface in the vector space. On the contrary, values of the third invariant $I_3(\mathsf{D})$ of the deviator and the first invariant $I_1(\mathsf{T})$ of the tensor are not constant but functions of orientation in the vector space. Thus, the distributions of $I_3(\mathsf{D})$ and $I_1(\mathsf{T})$ on the surface of unit sphere in the vector space are discussed in the following.

A reduced value $\bar{I}_3(\mathsf{D}_e)$ of the third invariant $I_3(\mathsf{D}_e)$ of the strain deviator D_e by means of the second invariant $I_2(\mathsf{D}_e)$ may be expressed in terms of the components e_i ($i=1, 2, 3$) of the deviatoric strain vector $\mathbf{e}$ as follows:

$$\bar{I}_3(\mathsf{D}_e)=\{e_1(e_1^2-3e_2^2)+(3/2)(e_1+\sqrt{3}\,e_2)e_3^2\}/(e_1^2+e_2^2+e_3^2)^{3/2}= \tag{5.1}$$

$$=\sin\theta_e\{\sin^2\theta_e\cos 3\varphi_e+3\cos^2\theta_e\cos(\varphi_e-\pi/3)\}.$$

As found from Eq. (5.1) the distribution of $\bar{I}_3(\mathsf{D}_e)$ in the space V_{3e} depends only on the orientation and may be expressed by the curves on the unit sphere in Fig. 2 obtained as intersections of Eq. (5.1) and the surface of the unit sphere $e_1^2+e_2^2+e_3^2+=1$.

The projections of these curves $\bar{I}_3(\mathrm{D}_e)$ onto the plane $-e_1 e_2$ become a set of straight segments shown in Fig. 3 with the dashed lines in the range $-1 \leqslant e_1 + \sqrt{3} e_2 \leqslant 1$, and may be expressed by one of the solutions of the following cubic equations obtained by eliminating e_3 from $e_1^2+e_2^2+e_3^2=1$ and Eq. (5.1):

$$(e_1+\sqrt{3}\,e_2)^3-3(e_1+\sqrt{3}\,e_2)+2\bar{I}_3(\mathrm{D}_e)=0\,.$$

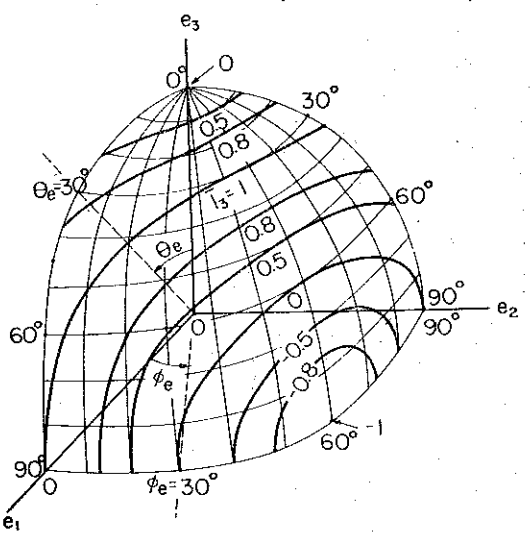

FIG. 2. Distribution of $\bar{I}_3(\mathrm{D})$ in the vector space V_{3e}.

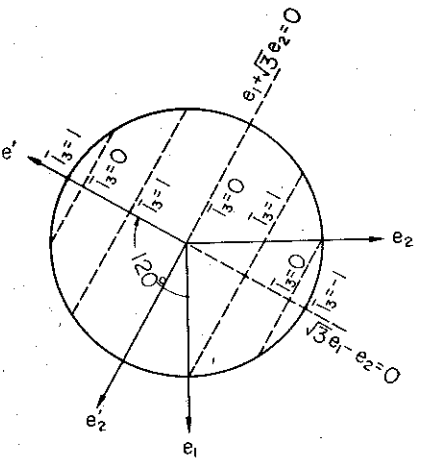

FIG. 3. Projection of the curves $\bar{I}_3(\mathrm{D})=$ $=$const on the plane $e_1 e_2$.

The solutions satisfying the condition $-1 \leqslant e_1+\sqrt{3e_2} \leqslant 1$ are found as follows:

$$e_1+\sqrt{3}\,e_2=-2\cos(2\pi/3-\alpha_e)\,,$$

where

$$\alpha_e=(1/3)\cos^{-1}\{\bar{I}_3(\mathrm{D}_e)\}\,. \tag{5.2}$$

On the other hand, the curves $\bar{I}_3(\mathrm{D}_e)$ on the spherical surface are projected as a set concentric circles on the plane $e_1+\sqrt{3}\,e_2=0$.

In the same manner the reduced value $\bar{I}_3(\mathrm{D}_\sigma)$ of the third invariant of the stress deviator D_σ may be expressed by the components σ_i $(i=1, 2, 3)$ of the deviatoric stress vector $\boldsymbol{\sigma}$ as follows:

$$\begin{aligned}\bar{I}_3(\mathrm{D}_\sigma)=3\sqrt{6}\,I_3(\mathrm{D}_\sigma)/I_2(\mathrm{D}_\sigma)^{3/2}=\{\sigma_1(\sigma_1^2-3\sigma_2^2)+(3/2)(\sigma_1+\sqrt{3}\,\sigma_2)\sigma_3^2\}/(\sigma_1^2+\\ +\sigma_2^2+\sigma_3^2)^{3/2}=\sin\theta_\sigma\{\sin^2\theta_\sigma\cos 3\varphi_\sigma+3\cos^2\theta_\sigma\cos(\varphi_\sigma-\pi/3)\}\,.\end{aligned} \tag{5.3}$$

The distribution of $\bar{I}_3(\mathrm{D}_\sigma)$ may be expressed by a set of dashed curves on the surface of unit sphere as shown in Fig. 4, as the intersections of $\sigma_1^2+\sigma_2^2+\sigma_3^2=1$ and Eq. (5.3).

The first invariant $I_1(\mathbf{T}_\sigma)$ of the stress tensor $\mathbf{T}_\sigma=\sigma_{ij}\,\mathbf{e}_i\,\mathbf{e}_j$ $(ij=1, 2, 3)$ is expressed as follows:

$$I_1(\mathbf{T}_\sigma)\equiv \mathrm{tr}(\mathbf{T}_\sigma)=\sigma_{11}+\sigma_{22}+\sigma_{33}. \tag{5.4}$$

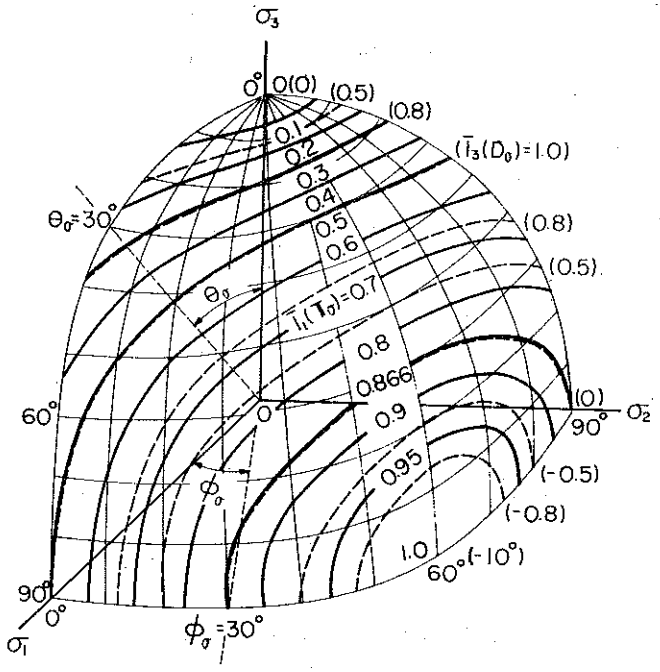

FIG. 4. Distribution of $I_3(\mathbf{D}_\sigma)$ and $I_1(\mathbf{T}_\sigma)$ in the space $V_{3\sigma}$.

Since the plane stress state $(\sigma_{33}=0)$ may be assumed in the thin-walled tubular specimen, $I_1(\mathbf{T}_\sigma)$ may be approximated as follows in considering Eq. (4.12).

$$I_1(\mathbf{T}_\sigma)=\sigma_{11}+\sigma_{22}=\sigma_1+\sqrt{3}\,\sigma_2. \tag{5.5}$$

The dimensionless value $I_1(\mathbf{T}_\sigma)$ reduced by the second invariant $I_2(\mathbf{D}_\sigma)$ is expressed as

$$\bar{I}_1(\mathbf{T}_\sigma)=(1/2)\,I_1(\mathbf{T}_\sigma)/\{3I_2(\mathbf{D}_\sigma)\}^{1/2}=(\sigma_1+\sqrt{3}\,\sigma_2)/(2|\boldsymbol{\sigma}|)= \\ =\sin\theta_\sigma\cos(\varphi_\sigma-\pi/3). \tag{5.6}$$

The distribution of $\bar{I}_1(\mathbf{T}_\sigma)$ in the space $V_{3\sigma}$ may be expressed by a set of solid curves on the surface of the unit sphere as shown in Fig. 4. The following relation is obtained from Eqs. (5.3) and (5.6) between $\bar{I}_3(\mathbf{D}_\sigma)$ and $\bar{I}_1(\mathbf{T}_\sigma)$ in the space $V_{3\sigma}$.

$$\bar{I}_3(\mathbf{D}_\sigma)=-4\bar{I}_1(\mathbf{T}_\sigma)\{\bar{I}_1(\mathbf{T}_\sigma)+\sqrt{3}/2\}\{\bar{I}_1(\mathbf{T}_\sigma)-\sqrt{3}/2\}. \tag{5.7}$$

It is found from Eq. (5.7) that the values $\bar{I}_1(\mathbf{T}_\sigma)=0,\ \pm\sqrt{3}/2$ correspond to $\bar{I}_3(\mathbf{D}_\sigma)=0$, and the value $\sqrt{3}/2$ is close to the extreme value $\bar{I}_1(\mathbf{T}_\sigma)=1$. As shown in Fig. 4, the following conditions exist:

$$\begin{aligned} &\bar{I}_1(\mathbf{T}_\sigma)=\sqrt{3}/2, \quad \bar{I}_3(\mathbf{D}_\sigma)=0 \quad \text{along the axis-}\sigma_2, \\ &\bar{I}_1(\mathbf{T}_\sigma)=0, \quad\ \ \bar{I}_3(\mathbf{D}_\sigma)=0 \quad \text{along the axis-}\sigma_3. \end{aligned} \tag{5.8}$$

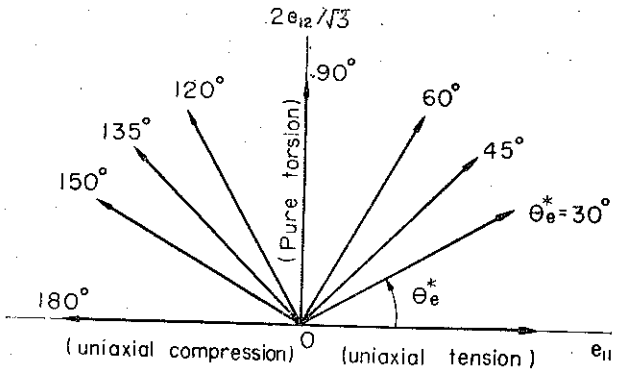

FIG. 5. Deviatoric strain vector space $V_2\,e$ for combined loads of axial force and torque.

6. PROPORTIONAL DEFORMATION TEST

6.1. Proportional deformation test in the plane -e_1 e_3 (V_{2e} for $\varphi_e=0$)

Figure 5 shows the vector space V_{2e} $(e_{11}, 2e_{12}/\sqrt{3})$ corresponding to the combination of tension and torque. The strain trajectories are shown by the radial lines starting from the origin (state of zero strain). The angle θ_e^* determines a ratio of deviatoric axial and shear strains (θ_e corresponds to a complementary angle of θ_e), and $\theta_e^*=0°, 90°$ and $180°$ correspond to the uniaxial tension, pure torsion and uniaxial compression, respectively. In the experiment, a constant strain rate $(ds/dt=3\times10^{-6}/\text{sec})$ was used, where s denotes an arc length of strain trajectory expressed by $s=\int(d/|e|/dt)\,dt$ in general. A plastic part of the arc length may be expressed by s^p.

In Fig. 6 the local stress space $V_{2\sigma}$ is shown at a point on the strain trajectory whose base vectors agree with those of V_{2e}.

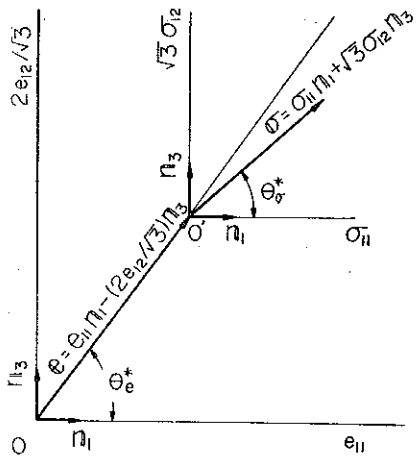

FIG. 6. Local vector space $V_{2\sigma}$ for deviatoric stress at a point on the strain trajectory.

6.1.1. $|\sigma|$-s^p curves

The resuts of the expreriment are expressed in the plane of deviatoric plastic strain $V_{2e}^p\,(e_{11}^p, 2e_{12}^p/\sqrt{3})$, where e_{11}^p and e_{12}^p denote the plastic parts obtained by subtracting the corresponding elastic parts from e_{11} and e_{12} by an assumption of the constant elastic moduli during plastic deformation.

The results of the proportional deformation test under combination of axial force and torque are shown in Fig. 7 for mild steel. As found from the figure, the curve for pure torsion ($\theta_e^*=90°$, $\bar{I}_3(D_e)=0$) appears lowest and the curves become

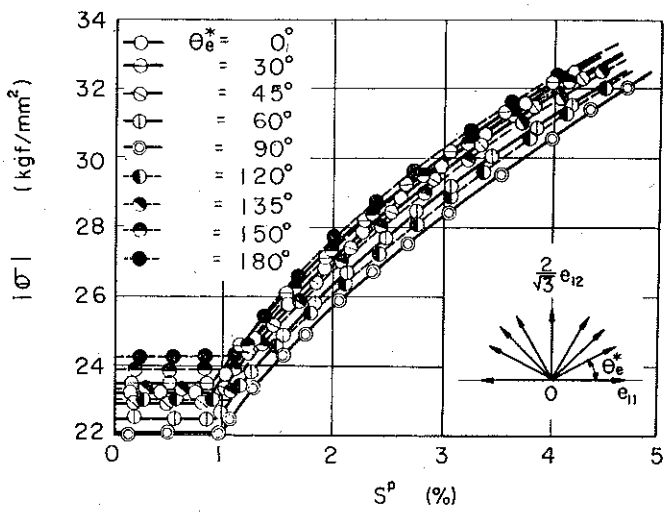

FIG. 7. $|\sigma|-s^p$ curves of proportional deformation under combined loads of axial force and torque.

higher with an increase of the axial strain (or stress) component, and the corresponding curves in the hardening region are close to each other for each pair of strain trajectories which are symmetric with respect to the axis $2e_{12}^p/\sqrt{3}$ (or $\sqrt{3}\,\sigma_{12}$), although the curves on the compression side ($90°<\theta_e^*\leqslant 180°$) appear a little higher than those on the tension side ($0°\leqslant\theta_e^*\leqslant 90°$) and the trend is more pronounced on the horizontal yield region.

6.1.2. *Relation between θ_σ^* and θ_e^**

The angles θ_σ^* and θ_e^* are expected to agree with each other for every proportional deformation. However, the experimental results proved that these angles did not always do so. They agree with each other for $\theta_e^*=0°$ and 180°, but the angle θ_σ^*

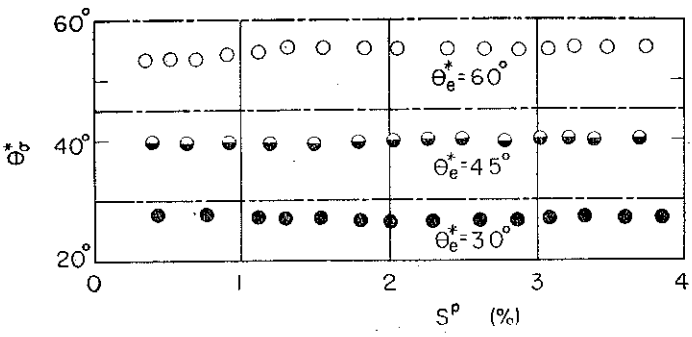

FIG. 8. Relation between the angles θ_e, θ_σ and s^p.

is smaller on the tension side and larger on the compression side than the angle θ_e^*. As shown in Fig. 8, the values of $|\theta_e^*-\theta_\sigma^*|$ remain almost constant at less than 5°.

6.1.3. Equi-strain curves [15], [16], [20].

In order to clarify the effect of $I_3(D_e)$ on the experimental results, equi-strain curves are described from the experimental results in Fig. 9. In the figure the small circles corresponding to the experimental results are connected by the solid curves.

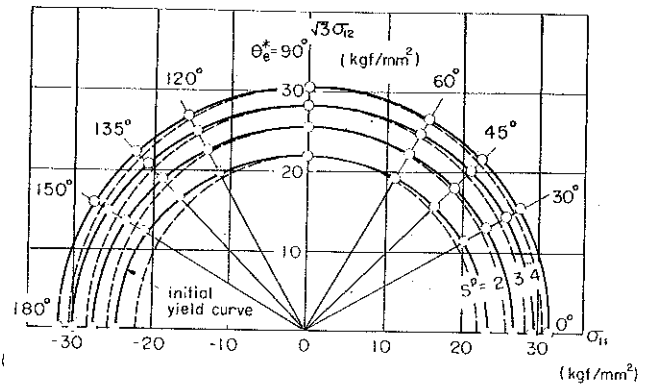

FIG. 9. Equi-strain curves.

The dashed curves show Mises' circle passing through the experimental points in pure torsion ($I_3(D_e)=0$) which correspond to the equi-strain curves without the effect of $I_3(D_e)$.

These equi-strain curves may be approximated with high accuracy by the following ellipse:

$$\{\sigma_{11}(s^p)/\sigma(s^p)\}^2+[\sqrt{3}\,\sigma_{12}(s^p)/\{\sqrt{3}\,\tau(s^p)\}]^2=1. \tag{6.1}$$

By introducing a modyfying coefficient

$$R_0=\sqrt{3}\,\tau(s^p)/\sigma(s^p), \tag{6.2}$$

the expression (6.1) is rewritten as follows:

$$\{R_0(s^p)\sigma_{11}(s^p)\}^2+\{\sqrt{3}\,\sigma_{112}(s^p)\}^2=\sqrt{3}\,\tau(s^p)\}^2, \tag{6.3}$$

where $\sigma(s^p)$ denotes the magnitude of the stress vector for uniaxial tension as a function of the arc length of the strain trajectory when the stress vector is in the first quadrant of the plane $(\sigma_{11}, \sqrt{3}\,\sigma_{12})$ and for uniaxial compression when the stress vector is in the second one, and $\sqrt{3}\,\tau(s^p)$ denotes that for pure torsion.

Equations (6.3) expresses a circle in a modified space with coordinate axes $R_0(s^p)\,\sigma_{11}(s^p)$ and $\sqrt{3}\,\sigma_{12}(s^p)$, whose radius corresponds to a modified, magnitude $|\boldsymbol{\sigma}^*|$ of the deviatoric stress vector. In the modified space every $|\boldsymbol{\sigma}|-s^p$ curve obtained in the experiment may be reduced to a curve $|\boldsymbol{\sigma}^*|-s^p$ corresponding to pure torsion

irrespective of the angle θ_e^*. In other words, by eliminating the effect of $\bar{I}_3(D_e)$ (or $\bar{I}_3(D_\sigma)$, because of the minute difference between $\bar{I}_3(D_e)$ and $\bar{I}_3(D_\sigma)$) from the experimental results, the deformation behaviour may be discussed as the relation between the second invariants of stress and strain deviators.

By expressing the modified magnitude $|\boldsymbol{\sigma}^*|$ as $R|\boldsymbol{\sigma}|$, the coefficient R is expressed as follows:

$$R=|\boldsymbol{\sigma}^*|/|\boldsymbol{\sigma}|=\{(R_0\sigma_{11})^2+3\sigma_{12}^2\}^{1/2}/(\sigma_{11}^2+3\sigma_{12}^2)^{1/2}= \\ =\{1+(R_0^2-1)\sin^2\theta_\sigma\}^{1/2}. \tag{6.4}$$

In the plane $(\sigma_{11}, \sqrt{3}\,\sigma_{12})$ with $\varphi_\sigma=0°$ a solution of Eq. (5.3) satisfying the condition $-1\leqslant\bar{I}_3(D_\delta)\leqslant 1$ is obtained as follows:

$$\sin\theta_\sigma=-2\cos\{2\pi/3-(1/3)\cos^{-1}\bar{I}_3(D_\sigma)\}. \tag{6.5}$$

By substituting Eq. (6.5) into (6.4), the following relation is obtained:

$$R=[1+4(R_0^2-1)\cos^2\{2\pi/3-(1/3)\cos^{-1}\bar{I}_3(D_\sigma)\}]^{1/2}. \tag{6.6}$$

In the three-dimensional space $V_{3\sigma}$, the following expression is obtained by substituting Eq. (5.3) into Eq. (6.6):

$$R=[1+4(R_0^2-1)\cos^2[2\pi/3-(1/3)\cos^{-1}\{\sin^3\theta_\sigma\cos 3\varphi_\sigma+ \\ +3\sin\theta_\sigma\cos^2\theta_\sigma\cos(\varphi_\sigma-\pi/3)\}]]^{1/2}, \tag{6.7}$$

where

$$R=\begin{cases}R_t=a(s^p)/b(s^p) & (0\leqslant\bar{I}_3(D_\sigma)\leqslant 1),\\ R_c=a(s^p)/c(s^p) & (-1\leqslant\bar{I}_3(D_\sigma)<0),\end{cases}$$

and $a(s^p)$, $b(s^p)$ and $c(s^p)$ denote the values of stress vector for pure torsion, uniaxial tension and uniaxial compression in relation to the arc length of the strain trajectory.

6.2. Proportionals deformation in the plane $-e_2\ e_3$ (V_{2e} *for* $\varphi_e=90°$)

Figure 10 shows the results of the proportional tests A ($\theta_e=0°$ along the axis-e_3), E ($\theta_e=32°$), F ($\theta_e=61.5°$) and G ($\theta_e=90°$ along the axis-e_2) for mild steel [15].

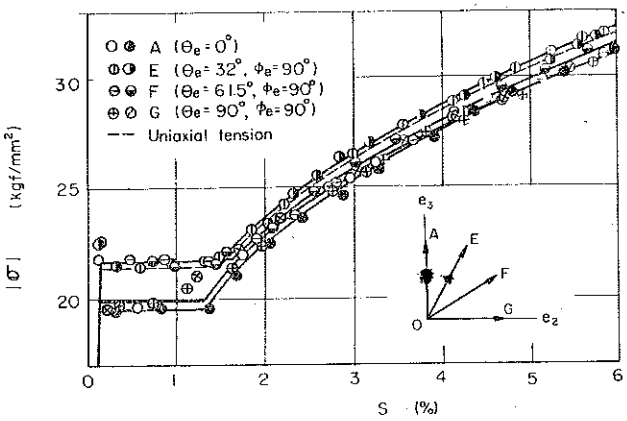

FIG. 10. Results of proportional deformation tests in the plane-$e_2\ e_3$.

In the figure, experimental points for the A-test along the axis-e_3 and those for the G-test along the axis-e_2 lie on an identical curve. The curve for the E-test corresponding to $\bar{I}_1=0.46$, $\bar{I}_3=0.99$ appears higher than that for the F-test corresponding to $\bar{I}_1=0.76$, $\bar{I}_3=0.52$. The difference between these curves suggests a possible effects of $\bar{I}_1$ (T_σ) as well as that of $\bar{I}_3$ (D_σ).

In order to estimate the effects of $\bar{I}_1$ and $\bar{I}_3$ on the deformation behaviour, proportional loadings along the axes σ_2 and σ_3 may be used because the values $\bar{I}_1=\pm\sqrt{3}/2$ and 0 along these axes differ markedly for the identical value of $\bar{I}_3=0$, as found from the conditions (5.8). On the other hand, the proportional deformation along the axes e_2 and e_3 may be regarded as those along the axes σ_2 and σ_3, respectively. Then the effect of $\bar{I}_1$ on the $|\boldsymbol{\sigma}|-s$ curves is found to be negligible from the above-mentioned results for the tests A and G along the axes e_3 and e_2. Therefore, it may be concluded that the difference between the $|\boldsymbol{\sigma}|-s$ curves due to the angle θ_e is the effect of $\bar{I}_3$ (D_σ).

7. Experimental results along the strain trajectories consisting of two straight branches

The plastic behaviour along the „strain trajectory with a right-angle corner" (symbolized as STN hereafter) may be discussed in the three-dimensional local vector space of the deviatoric stress $V_{3\sigma}$ established at a point on the STN in the

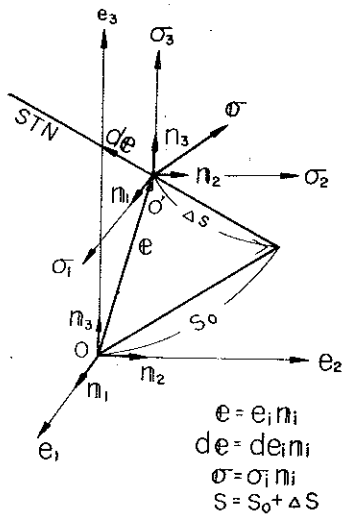

Fig. 11. Local stress space $V_3\,\sigma$ $(\sigma_1, \sigma_2, \sigma_3)$ on STN in the space V_{3e} (e_1, e_2, e_3).

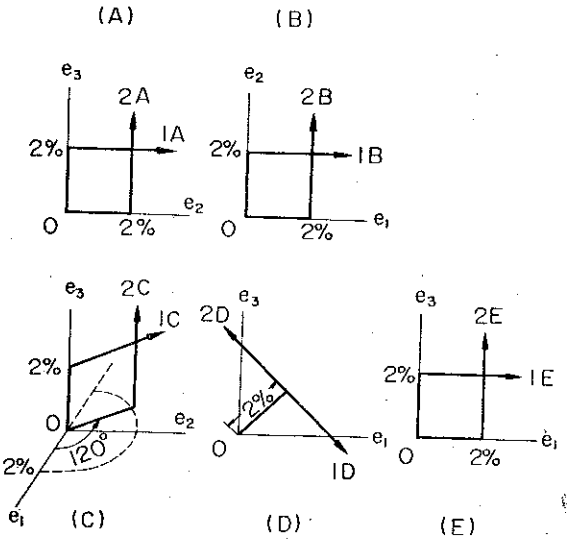

Fig. 12. STN used for experiments in the space V_{3e}.

three-dimensional vector space of the deviatoric strain V_{3e} shown in Fig. 11. In the figure, the length s_0 of the first branch corresponds to the pre-strain, $\Delta s=(s-s_0)$ shows a length of the second branch after the corner point, and $\mathrm{e}=e_i\,\mathrm{n}_i$, $d\mathrm{e}=de_i\,\mathrm{n}_i$

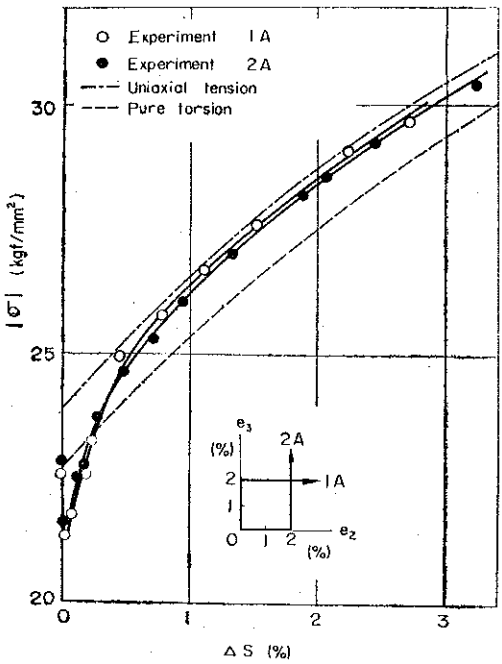

FIG. 13. $|\sigma|-\Delta s$ curves obtained by the 1*A* and 2*A* tests

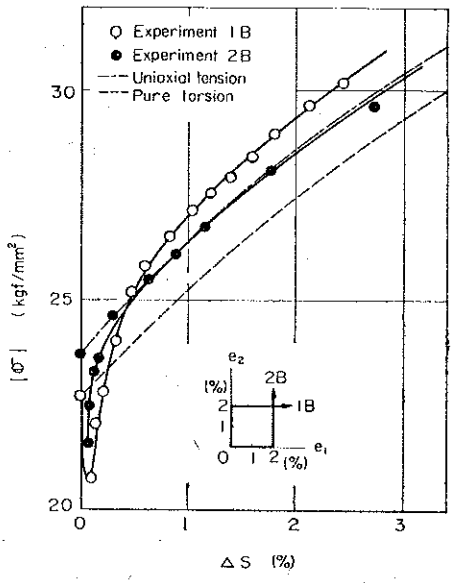

FIG. 14. $|\sigma|-\Delta s$ curves obtained by the 1*B* and 2*B* tests.

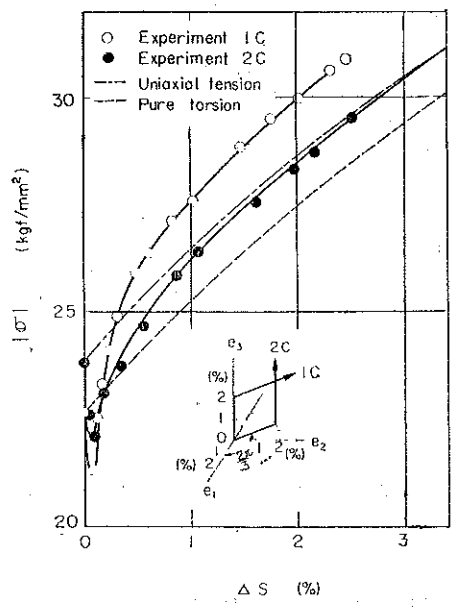

FIG. 15. $|\sigma|-\Delta s$ curves obtained by the 1*C* and 2*C* tests.

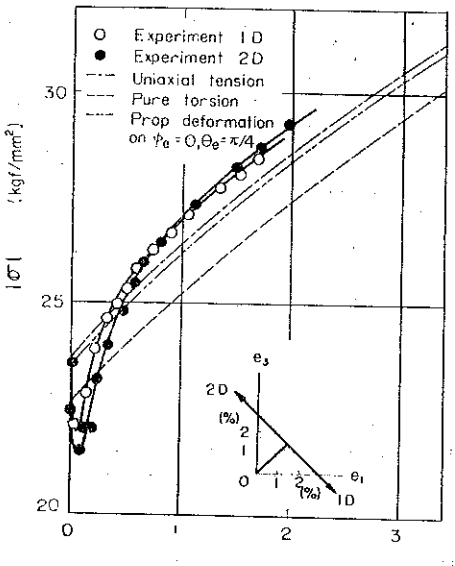

FIG. 16. $|\sigma|-\Delta s$ curves obtained by the 1*D* and 2*D* tests.

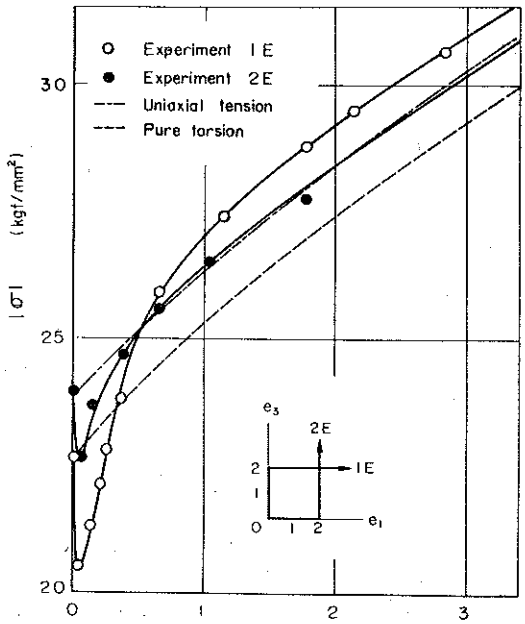

FIG. 17. $|\boldsymbol{\sigma}|-\Delta s$ curves obtained by the $1E$ and $2E$ tests.

and $\boldsymbol{\sigma}=\sigma_i \mathbf{n}_i$ denote the strain, strain-increment and stress vectors, respectively.

Experimental results are discussed on the STN's shown in Fig. 12 as well as in the Table. These results are obtained by apllying the combined loads of axial force, torque and internal pressure to the thin-walled tubular specimen of mild steel. Strain rate is kept constant ($ds/dt=3\times10^{-6}$/sec) in every test.

Table 1. STN tested for mild steel ($s_0=2$ percent)

Experiment		1A	2A	1B	2B	1C	2C	1D	2D	1E	2E
first branch	φ_e	90°	90°	90°	0°	120°	120°	0°	0°	0°	0°
	θ_e	90°	90°	0°	90°	120°	120°	0°	0°	0°	0°
second branch	φ_e	90°	0°	0°	0°	90°	0°	45°	45°	0°	90°
	θ_e	0°	90°	0°	0°	0°	90°	135°	−45°	90°	0°

7.1. $|\boldsymbol{\sigma}|-\Delta s$ curves

The curves obtained by the tests along the STN's $1A$, $2A$ through $1E$, $2E$ are shown in Figs. 13 through 17. The corresponding parts of the curves for pure torsion and uniaxial tension are indicated by the dashed and chain curves, respectively. A sudden drop in $|\boldsymbol{\sigma}|$ occurs just after the corner of STN in every experiment. This sudden drop occurs for increasing strain at constant rate, and thus cannot be regarded as the so-called unloading which has been defined with decreasing strain in the quasi-static process. This drop might be attributable to a stress relaxation effect,

because the strain along the first branch persists at the corner whereas the strain component along the second branch is very small. However, when the second branch is not present, the decrease of stress has been ascertained to attain only about one-third of the total decrease obtained above. Moreover, from the results obtained for the STN's in the e_1 e_2-plane, this stress decrease may be found in the deformation in which the principal stress axes do not rotate through the first and second branches of STN. Therefore, this phenomenon can be ascribed to a microscopic instability of materials induced by a change in microscopic structure (release of dislocation piled up during pre-strain, for example) just after a sudden change in strain (or stress) state. In other words, the comulative dislocation fixed during the deformation along the first branch is released as a result of the strain application in the direction of the second branch, and the resulting increase of plastic strain reduces the elastic part of the total strain which is increasing with constant rate. This can be related directly to the sudden drop in $|\sigma|$ mentioned above. The considered phenomenon may be regarded as a transitional one and cannot be discussed by means of the flow theory based mainly on Drucker's hypothesis on the premise of a stably hardening process.

As found from these figures, the curves $|\sigma|-\Delta s$ corresponding to the STN's which are in the relation of mirror transformation in V_{3e} do not always agree with each other. In line with the foregoing discussion, this may be attributed partly to

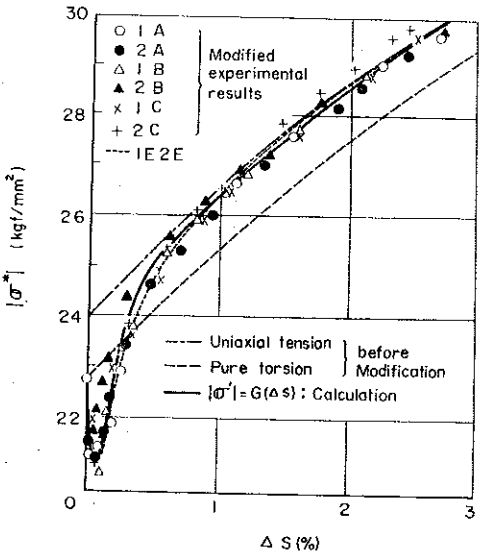

FIG. 18. Modified curves $|\sigma^*|-\Delta s$ obtained by using the coefficient R.

the effect of I_3 (D_e). For example, the curves $|\sigma|-\Delta s$ for the second branch of STN's agree well for the tests $1A$ and $2A$ along the axes e_2 and e_3 for which I_3 (D_e) have the same value 0.

Figure 18 shows an example of the curve $|\delta^*|-\Delta s$ modified by using the coefficient R introduced in the previous section. As shown in Fig. 18, the modified curve

$|\sigma^*| - \Delta s$ for which the remarkable difference was observed before modification for the STN's in the relation of mirror transformation is reduced to an identical curve after modification.

7.2. Angle θ between the strain-increment and stress vectors

In the results obtained by the tests of the strain-controlled type, the direction of the stress vector σ delays from that of the strain-increment vector which coincides with STN. The angle θ between the σ and de directions is expressed by $\theta = \cos^{-1}(\sigma \cdot$

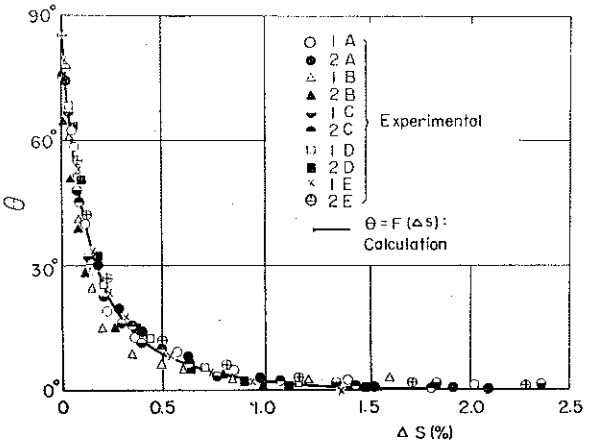

FIG. 19. Relation betwen θ and Δs.

$\theta de/|\sigma|\,|de|$. The value of θ varies with the increase of Δs. An example of the relation $\cdot - \Delta s$ is shown in Fig. 19 where the functions $\theta\,(\Delta s = F(\Delta s)$ are almost the same for every STN.

8. FORMULATION OF STRESS-STRAIN RELATION FOR THE SECOND BRANCH OF STN [16]

8.1. Equivalent strain trajectory in the space V_{3e}

From the discussion in Sect. 4 and its experimental verification for special case in Sect. 7, every strain trajectory oriented in the direction of $\bar{I}_3\,(D_e) = \text{const}$ is tensorially equivalent, whereas the corresponding stress state may be different. For example, equivalent strain trajectories for the strain trajectory $2E$, obtained by rotating the coordinate axes established in the element by an angle φ around the axis-3 (radial direction of the specimen), are shown with the thick solid lines in Fig. 20. In other words, a STN having the corner at arbitrary point on the circle $\bar{I}_3\,(D_e) = = \text{const}$ on the spherical surface, whose center lies at the origin, may represent all the trajectories having the corner on the circle.

On the other hand, since the plane $\sqrt{3}\,e_1 - e_2 = 0$ intersects with every circle mentioned above, as seen in Fig. 3, every STN having the corner on the spherical surface may be equivalent with either STN having its first branch in this plane.

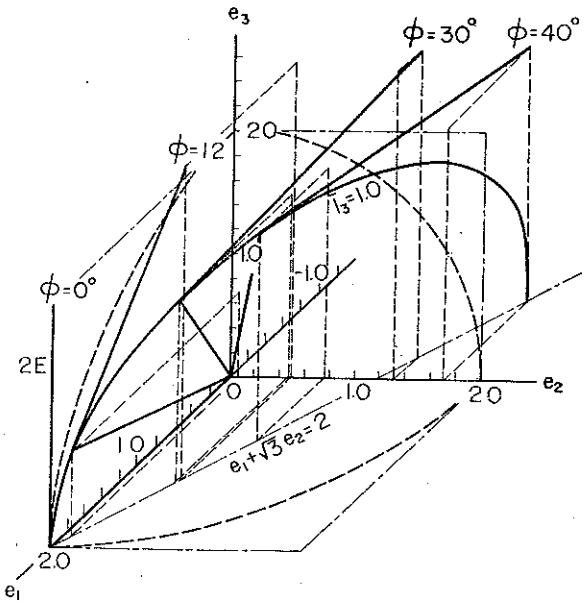

FIG. 20. STN's which are tensorially equivalent to STN for the 2E test.

When a coordinate system $e_1' e_2' e_3'$ (Fig. 3) is introduced by rotating the system $e_1 e_2 e_3$ 120° clockwise around the axis-3, the values of e_1', e_2' and e_3' may be expressed as follows:

$$e_1' = -(e_1 + \sqrt{3}\, e_2)/2 = -(e_{11} + e_{22}), \quad e_2' = (\sqrt{3}\, e_1 - e_2)/2 = \\ = (e_{11} - e_{22})/\sqrt{3}, \quad e_3' = e_3 = 2e_{12}/\sqrt{3}. \tag{8.1}$$

Since the plane $\sqrt{3}\, e_1 - e_2 = 0$ is expressed by the plane $e_1' e_3'$ in the system $e_1' e_2' e_3'$, every STN mentioned above may be replaced by a STN having its first branch in the plane-$e_1' e_3'$.

8.2. Stress-strain relation for STN *whose first branch lies in the plane-$e_1' e_3'$*

As shown in Fig. 21, a STN is considered in which the first branch makes an angle β to the axis-e_1' in the plane-$e_1' e_3'$, and the second branch makes an angle α to the plane-$e_1' e_3'$. Moreover, s_0 denotes the length of the first branch (pre-strain) and Δs denotes that of the second branch after the corner. When a local coordinate system $\sigma_1' \sigma_2' \sigma_3'$ whose axes are parallel with those of the previous system is established at a point on the second branch, the relations between σ_1', σ_2', σ_3' and σ_1, σ_2, σ_3 are expressed as follows:

$$\sigma_1' = -(\sigma_1 + \sqrt{3}\, \sigma_2)/2 = -3(s_{11} + s_{22})/2, \quad \sigma_2' = (\sqrt{3}\, \sigma_1 - \sigma_2)/2 = \\ = \sqrt{3}\, (s_{11} - s_{22})/2, \quad \sigma_3' = \sigma_3 = \sqrt{3}\, s_{12}. \tag{8.2}$$

The direction of the vector $d\mathbf{e}$ coincides with that of the second branch and the direction of $\boldsymbol{\sigma}$ delays by an angle θ from that of $d\mathbf{e}$ in the plane of STN. Therefore,

in order to formulate the stress-strain relation in the form of Eq. (3.12) it is necessary to determine the orthogonal rotation tensor L as well as the angle of the stress state α_σ and the intensity ζ_σ of the stress deviator D_σ.

8.2.1. Determination of angle α_σ

When the direction $\boldsymbol{\sigma}$ delays from that of $d\mathbf{e}$ by the angle $\theta\,(=F(\Delta s))$ at the length Δs after the corner, the following relations are obtained from Fig. 21:

$$
\begin{aligned}
\sigma_1' &= |\boldsymbol{\sigma}|\,(\sin\theta\cos\beta - \\
&\qquad -\cos\theta\cos\alpha\sin\beta), \\
\sigma_2' &= |\boldsymbol{\sigma}|\cos\theta\sin\alpha, \\
\sigma_3' &= |\boldsymbol{\sigma}|\,(\cos\theta\cos\alpha\cos\beta+\sin\theta\sin\beta).
\end{aligned}
\tag{8.3}
$$

Moreover, the following relation is obtained from Eqs. (5.3) and (8.2):

$$
\bar{I}_3(\mathsf{D}_\sigma)=\cos 3\alpha_\sigma=\sigma_1'(\sigma_1'^2-3\sigma_2^2- \\
-3\sigma_3'^2)/\sigma_1'^2+\sigma_2'^2+\sigma_3'^2)^{3/2}. \tag{8.4}
$$

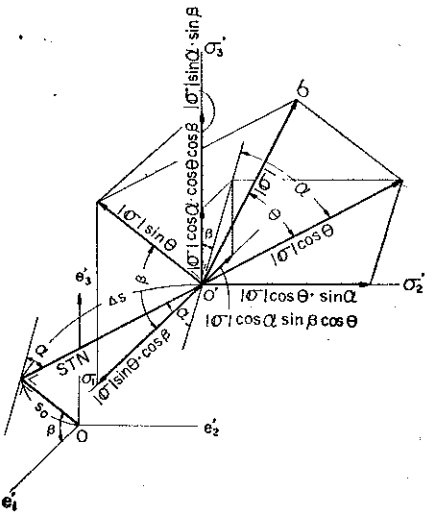

FIG. 21. Local stress vector space $V_{3\sigma}(\sigma_1', \sigma_2', \sigma_3')$ on STN in the space $V_{3e}(e_1', e_2', e_3')$.

By substituting the relations (8.3) into Eq. (8.4), α_σ is expressed as follows:

$$
\alpha_\sigma=(1/3)\cos^{-1}[(\sin\theta\cos\beta-\cos\theta\cos\alpha\cos\beta)\{(\sin\theta\cos\beta- \\
-\cos\theta\cos\alpha\sin\beta)^2-3\cos^2\theta\sin^2\alpha-3(\cos\theta\cos\alpha\cos\beta+\sin\theta\sin\beta)^2\}]. \tag{8.5}
$$

In the same way, as for the vector $d\mathbf{e}$, the following expressions are found from Fig. 21:

$$
de_1'=|d\mathbf{e}|\cos\alpha\sin\beta, \qquad de_2=|d\mathbf{e}|\sin\alpha, \qquad de_3'=|d\mathbf{e}|\cos\alpha\cos\beta. \tag{8.6}
$$

By substituting the relations (8.6) into the relation obtained from Eqs. (5.1) and (8.1), α_{de} is expressed as follows:

$$
\alpha_{de}=(1/3)\cos^{-1}\{-\cos\alpha\sin\beta(\cos^2\alpha\sin^2\beta-3\sin^2\alpha-3\cos^2\alpha\cos^2\beta)\}. \tag{8.7}
$$

8.2.2. Determination of the orthogonal rotation tensor L

There exist the following relations between the orthogonal rotation tensor $\mathsf{L}\ (=L_{ij}\,\mathbf{e}_i\,\mathbf{e}_j;\ i,j=1,2,3)$ and the rotation vector $\boldsymbol{\omega}=\omega_k\,\mathbf{e}_k$:

$$
\begin{aligned}
\mathsf{L} &= \exp e^{\omega\Omega}=\mathsf{I}+\boldsymbol{\Omega}\sin\omega+(1-\cos\omega)\,\boldsymbol{\Omega}^2, \\
\mathsf{L}^{-1} &= \exp e^{\omega\Omega}=\mathsf{I}-\boldsymbol{\Omega}\sin\omega+(1-\cos\omega)\,\boldsymbol{\Omega}^2.
\end{aligned}
\tag{8.8a}
$$

and

$$
\mathsf{I}=\delta_{ij}\,\mathbf{e}_i\,\mathbf{e}_j, \qquad \boldsymbol{\Omega}=\Omega_{ij}\,\mathbf{e}_i\,\mathbf{e}_j, \qquad \Omega_{ij}=(\alpha_{ij}-\alpha_{ji})/2, \qquad \alpha_{ij}=\mathbf{e}_{ijk}\,\alpha_k, \tag{8.8b}
$$

where ω denotes the magnitude (rotation angle) of $\boldsymbol{\omega}$, and α_k denotes the direction of $\boldsymbol{\omega}$ (direction cosine for the axis of rotation).

Along the second branch of STN, the magnitude ω is given as

$$\omega=\omega_\sigma-\omega_{de}, \tag{8.9a}$$

where

$$\tan 2\omega_\sigma=2s_{12}/(s_{11}-s_{22})= \tag{8.9b}$$

$$=-\sigma'_3/\sigma'_2=(\cos\theta\cos\alpha\cos\beta+\sin\theta\sin\beta)/\cos\theta\sin\alpha,$$

$$\tan 2\omega_{de}=2de_{12}/(de_{11}-de_{22})=de'_3/de'_2=\cos\alpha\cos\beta/\sin\alpha.$$

Since the axis of rotation coincides with the axis-3 (radial direction in the specimen) of the coordinate system established in the element, the above-mentioned relations may be reduced to the case $\alpha_1=\alpha_2=0$, $\alpha_3=1$, and thus

$$\boldsymbol{\Omega}=\mathrm{e}_1\mathrm{e}_2-\mathrm{e}_2\mathrm{e}_1, \quad \boldsymbol{\Omega}^2=-\mathrm{e}_1\mathrm{e}_1-\mathrm{e}_2\mathrm{e}_2. \tag{8.10}$$

By substituting Eqs. (8.9a), (8.9b) and (8.10) into Eqs. (8.8a), the orthogonal rotation tensor L may be obtained.

8.2.3. Determination of ζ_σ

The parameter ζ_σ expressing the intensity of D_σ is given in the following form:

$$\zeta_\sigma(\Delta s)=|\boldsymbol{\sigma}|/\sqrt{3}=|\boldsymbol{\sigma}^*|/\sqrt{3}\,R=G(\Delta s)/\sqrt{3}\,R, \tag{8.11}$$

where R is given by Eq. (6.6). Since the expression $\{\cos^{-1}I_3(\mathrm{D}_\sigma)\}/3$ in Eq. (6.6) corresponds to α_σ given in Eq. (8.5), if the functional form $\alpha_\sigma(\Delta s)$ in Eq. (8.5) is obtained from the experimental results, $\alpha_\sigma(\Delta s)$ may be found with the use of $G(\Delta s)$.

The relation between D_σ and D_{de} may be obtained by substituting these parameters into Eq. (3.12). From the relation thus obtained, the stress deviator D_σ may be calculated along the second branch of STN whose first branch lies in the plane-$e'_1\,e'_3$.

8.3. Stress-strain relation for STN of arbitrary orientation

Stress-strain relation along the second branch of STN, whose first branch starts at the origin (state of zero strain) and the second branch intersects with the first branch normally, may be determined by selecting the corresponding angle α and β in Fig. 22 in the following way.

If a strain vector on the first branch and a strain-increment vector on the second one are expressed by $\mathrm{e}_a=e^a_i\,\mathrm{n}'_i$ and $d\mathrm{e}_b=de^b_i\,\mathrm{n}'_i$, where n'_i denotes the base vector of the axis-e'_i, respectively, the following condition holds:

$$\mathrm{e}_a\cdot d\mathrm{e}_b=0. \tag{8.12}$$

One of the STN's equivalent with the above-mentioned STN, whose first branch lies in the plane-$e'_1\,e'_3$, is shown in Fig. 22 with the dashed line. In the same figure the relation

$$\cos\beta=\mathrm{n}'_1\cdot\mathrm{e}_a/|\mathrm{n}'_1|\,|\mathrm{e}_a|=e^a_1/|\mathrm{e}_a| \tag{8.13}$$

may be found. From the relation $\mathbf{AB}=\mathrm{e}_a-\mathbf{OA}=\mathrm{e}_a-|\mathrm{e}_a|\,\mathrm{n}'_1/\cos\beta$, the following relation is obtained:

$$\cos\alpha=d\mathrm{e}_b\cdot\mathbf{AB}/|d\mathrm{e}_b|\,|\mathbf{AB}|=-de^b_1/|d\mathrm{e}_b|\sin\beta. \tag{8.14}$$

These relations are expressed in tensor components as follows:

$$\begin{aligned}\cos\beta&=-(e^a_1+e^a_{22})/(2e^a_{ij}\,e^a_{ij}/3)^{1/2},\\ \cos\alpha&=(de^b_{11}+\\ &\quad+de^b_{22})/(2de^b_{ij}\,de^b_{ij}/3)^{1/2}\sin\beta.\end{aligned} \tag{8.15}$$

8.4. Determination of the functional form of $|\boldsymbol{\sigma}^*|=G(\Delta s)$ *and* $\theta=F(\Delta s)$

On the second segment of the strain trajectory, the components of the stress vector parallel and perpendicular to the trajectory are designated as $G_1(\Delta s)$ and $G_2(\Delta s)$. Since the component of the stress vector perpendicular to the trajectory decays with the increase of Δs from the value at the corner, the functional from $G_2(\Delta s)$ may be expressed as

$$G_2(\Delta s)=22.75\,e^{-2.8\Delta s} \tag{8.16a}$$

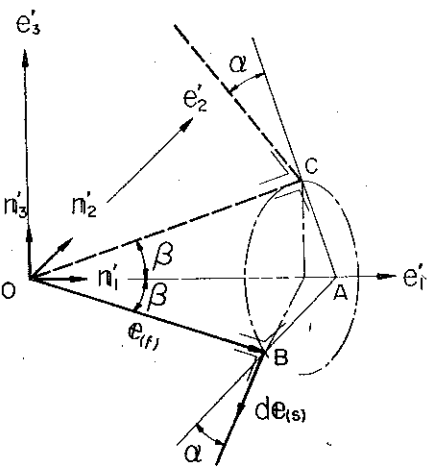

FIG. 22. Equivalent STN's in the space V_{3e}

from the experimental result shown in Fig. 18, where 22.75 kgf/mm^2 corresponds to the magnitude of the modified stress vector at the corner point.

On the other hand, the component of the stress vector parallel to the trajectory increases almost exponentially with the increase of Δs just after the corner, thus the form of $G_1(\Delta s)$ may be approximated by

$$G_1(\Delta s)=23.7(1-e^{-7.4\Delta s})+|3.63(\Delta s)^{0.7}-1.0|, \tag{8.16b}$$

where the second term on the right hand side modifies the function so that the experimental result may be approximated well for large values of Δs. This term does not affect significantly the value of $G(\Delta s)=|\boldsymbol{\sigma}^*|(\Delta s)$ at the corner ($\Delta s=0$) for the sufficiently large value of $G_2(\Delta s)$.

Then, the functional form of $G(\Delta s)$ is obtained from the following relation:

$$G(\Delta s)=\{G_1^2(\Delta s)+G_2^2(\Delta s)\}^{1/2}. \tag{8.16c}$$

The functional form of $\theta=F(\Delta s)$ obtained from the experimental result may be expressed as follows:

$$F(\Delta s)=30(2e^{-10\Delta s}+e^{-2.5\Delta s}). \tag{8.17}$$

The results for $|\boldsymbol{\sigma}^*|$ and θ calculated by Eqs. (8.16) and (8.17) are shown in Figs. 18 and 19 with solid curves, respectively. As found in these figures, the functions (8.16) and (8.17) are close approximations of the experimental results, respectively.

8.5. Results of calculation of stress-strain relation for concrete form of STN and comparison with the experimental result [20]

An example of the calculation is considered by using the above — obtained strain trajectories 2C and 2E (Figs. 15 and 17). These two trajectories are equivalent tensorially and correspond with the case of $\cos\alpha=0$ and $\cos\beta=-1/2$ as found from the relations (8.15).

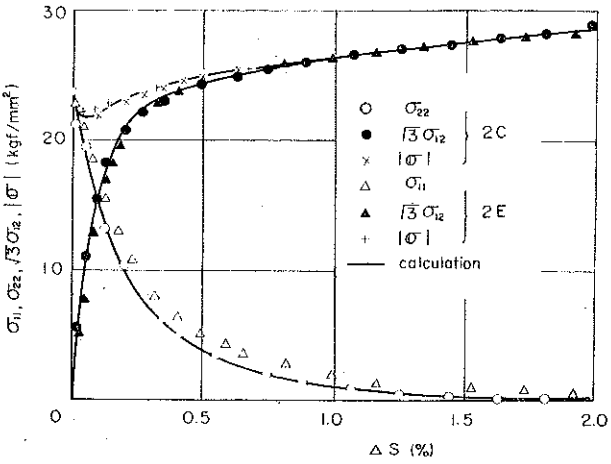

FIG. 23. Relation between the stress components and Δs calculated by a tensorial equation in comparing with the corresponding experimental results in the 2*C* and 2*E* tests

The results of calculation are shown in Fig. 23 with the solid curves. In the figure, various symbols show the corresponding experimental results. These solid curves approximate the experimental results with high accuracy, and almost the same degree of approximation can be obtained for other experimental results. Therefore, it may be concluded that the tensor equation (3.12) may approximate with high accuracy the stress-strain relation along the second branch of every STN in the set of STN's of fixed geometry, if the deformation characteristics of the material are measured along any STN.

Figure 24 compares the tensorially linear term on the right hand side of Eq. (3.12)

$$s_{11}^{L}=\{\zeta_\sigma \sin(2\alpha_{de}+\alpha_\sigma)/\sin 3\alpha_{de}\}(\mathsf{L}D_{de}\mathsf{L}^{-1}/\zeta_{de}) \tag{8.18a}$$

with the tensorially nonlinear term

$$s_{11}^{N}=\{\sqrt{3}\,\zeta_\sigma \sin(\alpha_{de}-\alpha_\sigma)/\sin 3\alpha_{de}\}(\mathsf{L}D_{de}^{2}\mathsf{L}^{-1}/\zeta_{de}^{2}-\sqrt{2/3}\,G_1) \tag{8.18b}$$

for their contributions to the axial stress component σ_{11} in the 2*B* test. As found from the figure, the contribution of the linear term is quite small and the component

σ_{11} consists of the tensorially nonlinear part just after the corner. However, the linear part increases while the nonlinear one decreases very quickly with the increase of Δs thereafter.

The reason why the σ_{11} curve in Fig. 24 has a hump just after the corner point may be explained as follows.

The value e_1 remains constant after the corner of the strain trajectory while the value σ_1 decreases from the magnitude $|\boldsymbol{\sigma}|$ at the corner point with the increase of Δs and tends to 0 for large values of Δs (Fig. 25). In other words, the value σ_1 varies so that the value of e_1 may be kept constant after the corner.

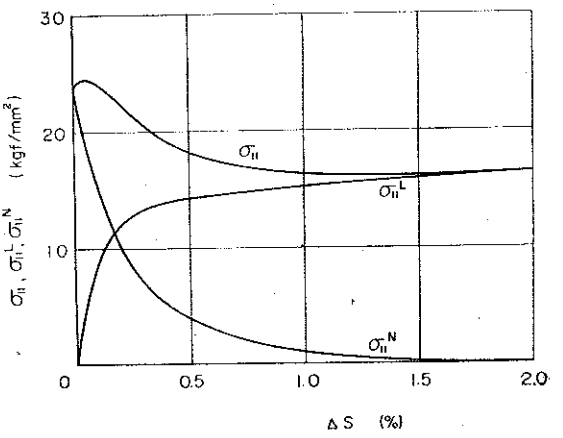

FIG. 24. Tensorially linear and nonlinear contributions for the stress components B_{11} in the $2B$ test

On the other hand, σ_1 and σ_2 are expressed by using the relation (4.13) as well as

$$s_{11}=\sigma_{11}-\sigma, \quad s_{22}=\sigma_{22}-\sigma, \quad \sigma_{33}=0,$$

as follows

$$\sigma_1=(2/3)s_{11}=(\sigma_{11}-\sigma_{22}/2), \quad \sigma_2=\sqrt{3}\,(s_{11}/2+s_{22})=\sqrt{3}\,\sigma_{22}/2.$$

Therefore, if the increasing rate of σ_{22} is larger than the decreasing rate of σ_1 with the increase of Δs, σ_{11} should increase to compensate the difference between these

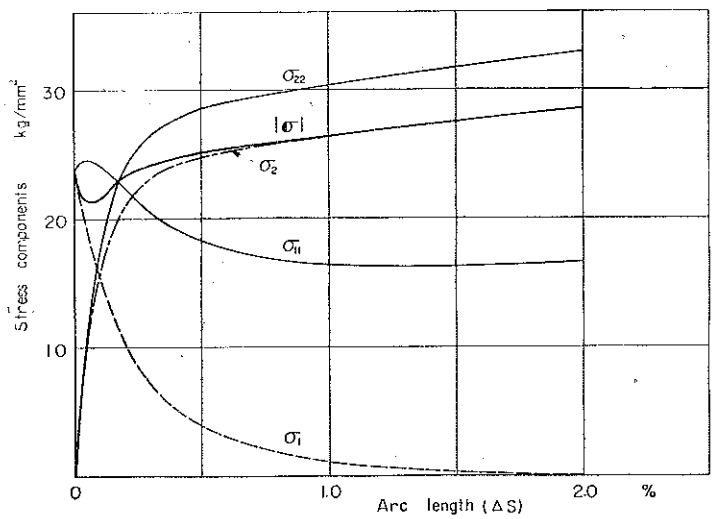

FIG. 25. Relation between the variation rates of $\sigma_{11}, \sigma_{22}, \sigma_1$ and σ_2 with respect to Δs

two rates. For all that, since the magnitude of the stress vector $\boldsymbol{\sigma}$ is obtained by the relation

$$|\boldsymbol{\sigma}|=(\sigma_1^2+\sigma_2^2)^{1/2}=\{(\sigma_{11}-\sigma_{22}/2)^2+3\sigma_{22}^2/4\}^{1/2},$$

$|\boldsymbol{\sigma}|$ may decrease with the increase of Δs in the range $\sigma_{11}\gg\sigma_{22}$ for the significant effect of σ_1 to the magnitude $|\boldsymbol{\sigma}|$.

The above-mentioned effect cannot be formulated by the conventional flow rule. However, in the range $\Delta s>1.0$ percent, since such an effect becomes negligibly small, the conventional stress-strain-increment relation may be a good approximation.

The phenomenon mentioned above, for example the drop of stress magnitude or the delay of the stress vector for the strain trajectory after the corner, should be understood as a transitional one appearing in the deformation under a constant strain rate. On the contrary, the results of a quasi-static test for this case using a stepwise loading increment seem to satisfy well the conventional flow rule. As a matter of fact, in such a quasi-static test the above-mentioned transient phenomenon occurs in the period in which the deformation and the corresponding stress attain a state of equilibrium on each loading step. When the measurement is not performed in this period, this phenomenon cannot be detected, and this may be why these transient phenomenons are not discussed in the results of quasi-static tests.

Judging from the fact that most of the deformation processes in engineering application are not of a quasi-static nature with stepwise load increment, the results of such a quasi-static test seem to be insufficient for analysing practical deformation state precisely.

9. Conclusion

We are trying to formulate the experimental results for arbitrarily prescribed configurations of a strain trajectory in the form of a nonlinear tensor equation. Though our study is not very profound at present, the following conclusions can be summarized from the above-mentioned discussions.

1) The third invariant of the strain (or stress) deviator affects the experimental results of plastic deformation of metal whereas the first invariant does little. Thus, the effect of the third invariant and the history effect on the deformation behaviour appears in the experimental results of the plastic deformation of mild steel under complex loading.

2) The first and third invariants in the isotropic tensor space cannot be invariants in the corresponding isotropic vector space. The distributions of the first and third invariants in the corresponding vector space depend on the orientation in the space. Since the vector space is convenient for discussing the deformation behaviour due to history effect, it seems promising to make use of the vector space in this discussion in modifying the experimental results so as to eliminate the effect of the third invariant.

3) For this purpose the effect of these invariants on the experimental results of plastic behaviour were discussed experimentally on the proportional deformation (constant values of these invariants) in the two-dimensional vector space, by applying

combined loads of axial force and torque to the thin-walled tubular specimen. In the results it was found that the effect of the third invariant on the experimental results may be eliminated by means of a comparatively simple procedure.

4) In order to expand the above-mentioned modification into the three-dimensional vector space, a modifying coefficient R was introduced. It was ascertained that the stress-strain curve for every proportional deformation in the three-dimensional vector space may be presumed from the experimental results obtained under the axial force and torque with the use of the coefficient R.

5) The plastic behaviour of mild steel after the corner of a strain trajectory consisiting of two straight segments which intersect with the right-angle corner was observed with high accuracy for each couple of trajectories, with a pre-strain 2 percent, which are in the relation of mirror image mutually. In the results a sudden drop in stress value was observed just after the corner for increasing strain at constant rate. The amount of stress drop is far larger than that corresponding to the stress relaxation for the strain component at the end of the first branch, which is kept constant after the corner. This phenomenon can be ascribed to a microscopic instability induced by a change in the microscopic structure of the materials at the sudden change in strain (or stress) state.

6) The sudden drop in stress value at the corner recovers quickly with an increase of strain, and the deformation curve $|\sigma| - \Delta s$ (or $|\sigma| - \Delta s^p$) after the recovery runs parallel with that of proportional deformation corresponding to the second branch. The range from the corner to the end of recovery is a transient one in which the history effect appears strongly.

The direction of the stress vector on the second branch delays markedly from that of the strain-increment vector just after the corner, but the delay disappears quickly with an increase of strain and, at about 1 percent of strain after the corner, both vectors may be regarded as to agree with each other. This transient range almost agrees with the range of recovery of stress drop after the corner.

The deformation curves after the recovery corresponding to the couple of strain trajectories which are in the relation of the mirror image do not agree with each other. In other words, the postulate of isotropy proposed by Ilyushin does not hold with high accuracy in the experimental results.

7) If the effect of the third invariant is eliminated from the experimental results with the use of the coefficient R, on the modified deformation curve after the transient range, the postulate of isotropy holds accurately for mild steel.

8) A general form of a non-linear tensorial equation between the stress and strain-increment deviators was derived to formulate the stress-strain relation along the second branch of a strain trajectory for mild steel for which the postulate of isotropy holds after modification. In this equation the stress deviator is expressed as a function of the strain-increment deviator.

In this case, since the principal axes of both deviators are not coaxial in the transient range, the equation was derived with respect to the principal axis of the stress deviator by operating an orthogonal rotation tensor upon the strain-increment

deviator. In this equation the functional expressing the history effect may be determined from the experimental results.

9) The stress-strain relation obtained above was confirmed to approximate accurately the experimental results of the plastic behaviour of mild steel after the corner.

10) In order to confirm the generality of the procedure in formulating stress--strain relation in this paper, some kinds of experiments have already been performed on brass and aluminium alloys (f.c.c. metals; on the contrary, mild steel is a b.c.c. one) and these results showed that the procedure could be suitable for brass, but not so suitable for aluminium alloys due to the effect of aging occurring on the deformation process at constant strain rate.

10. Acknowledgements

The author should like to express his sincere thanks to Professor A. Sawczuk and Professor Z. Mróz and other scientists in the Polish Academy of Sciences for their very kind arrangements to invite him to one of the general lectures at the 18th Polish Solid Mechanics Conference. The author also wishes to express his hearty thanks to Professor A. A. Ilyushin and Professor V. S. Lensky and other scientists from the Moscow State University as well as to Professor L. M. Kachanov and Professor A. A. Bakulenko from the Leningrad State University for their very helpful discussion and instructive comments on the results of our investigations.

References

1. R. Hill, *The mathematical theory of plasticity*, Oxford University Press 1950.
2. W. Prager, Proc. Intern. Mech. Engrs., **169**, 41, 1955.
3. H. Ziegler, Q. Appl. Mech., **17**, 55, 1959.
4. A. Baltov and A. Sawczuk, Acta Mech., **1**, 81, 1965.
5. Z. Mróz, J. Mech. Phys. Solids, **15**, 163, 1967.
6. G. Backhaus, Zeit. angew. Math. Mech., **48**, 99, 1968.
7. A. A. Eisenberg and A. Phillips, Acta Mech., **5**. 1, 1969.
8. J. F. Williams and N. L. Svenson, J. Strain Analysis, **5**, 128, 1970.
9. C. Truesdell and W. Noll, *The nonlinear field theories of mechanics*, Encyclopedia of Physics, III, 3, 1965.
10. A. A. Ilyushin, Appl. Math. Mech., **18**, 641, 1954 [in Russian]; *Problems in the theory of plasticity*, Acad. Sci. USSR, 1961, [in Russian]; *Plasticity*, Foundation of General Mathematical Theory, Acad. Sci. USSR, 1963 [in Russian].
11. V. S. Lensky, *Plasticity*, Proc. 2nd Symp. on Naval Struc. Mech., **259**, Pergamon 1960.
12. D. D. Ivlev, Trans. Acad. Sci. USSR, **2**, 1960 [in Russian].
13. V. V. Novozhilov, Trans. Acad. Sci. USSR, **3**, 1961 [in Russian].
14. Y. Ohashi and M. Tokuda, J. Mech. Phys. Solids, **21**, 241, 1973.
15. Y. Ohashi, M. Tokuda and H. Yamashita, J. Mech. Phys. Solids, **23**, 295, 1975.
16. Y. Ohashi, M. Tokuda and Y. Tanaka, J. Mech. Phys. Solids, **25**, 1977.

17. A. A. BAKULENKO, *Study on elasticity and plasticity*, Leningrad University Press, **8**, 3, 1971 [in Russian].
18. Y. OHASHI and K. KAWASHIMA, J. Mech. Phys. Solid, 25, 1977.
19. Y. OHASHI, M. TOKUDA and Y. TANAKA, (to be submitted to a journal of Polish Acad. Sci.)
20. Y. OHASHI, K. KAWASHIMA and N. MORI, Trans. ASME, J. Eng. Mat. Tech., **98**, 282, 1976.

STRESZCZENIE

DOKŁADNE POMIARY I OPIS PLASTYCZNEGO ZACHOWANIA SIĘ METALI

W niniejszej pracy podsumowano wyniki badań dotyczących plastycznego zachowania się metali w warunkach złożonego obciążenia, przeprowadzonych na automatycznej maszynie testującej dla złożonego obciążenia, na podstawie danych otrzymanych w naszym laboratorium. Przedyskutowano kilka wyników doświadczalnych dla miękkiej stali, poddanej proporcjonalnym deformacjom w warunkach złożonego obciążenia przy jednoczesnym działaniu siły osiowej, momentu skręcającego i ciśnienia wewnętrznego. Doświadczenia przeprowadzono na cienkościennych rurkowych próbkach przy stałej prędkości odkształcenia, kładąc nacisk na wpływ drugiego i trzeciego niezmiennika naprężenia i odkształcenia.

Dyskusję wyników eksperymentalnych przy wspomnianych wyżej złożonych obciążeniach przeniesiono następnie na plastyczne zachowanie się materiału wzdłuż trajektorii odkształcenia z prostokątnym narożem w trójwymiarowej przestrzeni wektorowej, odpowiadającej dewiatorowi odkształcenia.

Z doświadczeń tych wynika, że związki między naprężeniem i odkształceniem za narożem trajektorii odkształcenia, które są w relacji z lustrzanym przekształceniem, nie zawsze są zgodne. Jednakże rozbieżność związków prawie zanika po modyfikacji, w której efekt trzeciego niezmiennika jest wyeliminowany z wyników doświadczalnych. Innymi słowy, po takiej modyfikacji wyników otrzymanych za pomocą wyżej wspomnianych doświadczeń dla miękkiej stali, «postulat o izotropii» Iljuszyna jest spełniony prawie całkowicie.

Po tej modyfikacji relacje doświadczalne między naprężeniem i odkształceniem za narożem trajektorii odkształcenia są sformułowane w postaci równości tensorowej.

Резюме

ТОЧНЫЕ ИЗМЕРЕНИЯ И ОПИСАНИЕ ПЛАСТИЧЕСКОГО ПОВЕДЕНИЯ МЕТАЛЛОВ

В настоящей работе подытожены результаты исследований, касающиеся пластического поведения металлов в условиях сложного нагручения, проведенных на автоматической испытательной машине для сложного нагружения на основе данных полученных в нашей лаборатории. Обсуждено несколько экспериментальных результатов для мягкой стади, подвергнутой пропорциональным деформациям в условиях сложного нагружения, при одновременном действии осевой силы, скручивающего момента и внутреннего давления. Эксперименты проведены на тонкостенных трубчатых образцах, при постоянной скорости деформации, подчеркивая влияние второго и тертьего инвариантов напряжения и деформации. Обсуждение экспериментальных результатов, полуленных при упомянутых выше сложных нагружениях, перенесено затем на пластическое поведение материала вдоль траектории деформации с прямоугильным ребром в трехмерном векторном пространстве, отвечающем девиатору деформации. Из этих экспериментов следует, что соотношения между напряжением и деформацией за ребром траектории деформации, которые связаны с зеркальным преобразованием, не всегда совпадают. Однако расходимость соотношений почти исчезает после модификации, в которой эффект третьего инварианта исключен из экспериментальных результатов. Иными

словами после такой модификации полученных результатов при помощи выше упомянутых экспериментов для мягкой стали, „постулат об изотропии" Ильюшина удовлетворяется почти полностью. После этой модификации экспериментальные соотношения между напряжением и деформацией за ребром траектории деформации сформулированы в виде тензорного равенства.

DEPARTMENT OF MECHANICAL ENGINEERING,
FACULTY OF ENGINEERING NAGOYA UNIVERSITY

Received March 24, 1977.